Applied Catalysis B: Environmental 304 (2022) 120948

Contents lists available at ScienceDirect

Applied Catalysis B: Environmental

journal homepage: www.elsevier.com/locate/apcatb

An oxygen carrier catalyst toward efficient chemical looping-oxidative coupling of methane

Weidong Sun, Guofeng Zhao, Ya Gao, Jiaqi Si, Ye Liu, Yong Lu *

Shanghai Key Laboratory of Green Chemistry and Chemical Processes, School of Chemistry and Molecular Engineering, East China Normal University, Shanghai 200062, China

ARTICLE INFO

Keywords:
Chemical looping
Oxidative coupling of methane
Ethylene
Oxygen carrier catalyst
Red-ox cycle

ABSTRACT

Chemical looping concept paves way toward intrinsically safe and efficient oxidative coupling of methane (CL-OCM) process, because it permits the reaction to proceed via repeating reduction-oxidation cycle in two reactors. It is calling for a ground-breaking catalyst with enough high selective CH_4-converting lattice-oxygen carrying capacity but represents a grand challenge. Herein, we report an efficient catalyst obtainable by decorating an oxygen carrier $FeMnO_3$ with Na_2WO_4, with good cycling performance, achieving a high space time yield of 29.8 $g_{C2\text{-}C3}$ $kg_{cat.}^{-1}$ h^{-1} with 20% CH_4 conversion and 80% C_2-C_3 selectivity at 800 °C and a low catalyst/CH_4 weight ratio of 13.5. CL-OCM process is established by "$FeMnO_3 \leftrightarrow [MnFe_2O_4 + MnO]$" redox cycle. Na_2WO_4-decoration gets lattice oxygen stored in $FeMnO_3$ transformed from non-selective to selective due to mitigation of lattice-oxygen evolution. Scaled up CL-OCM testing with 10-gram catalyst also yields comparable results seen in the case of using 1-gram catalyst, validating great application potential.

1. Introduction

Light olefins are the basic building blocks in modern petrochemical industry; in particular, ethylene is the largest volume olefin used as the monomer of polyethylene and as the intermediate to produce ethylene dichloride, ethylene oxide, and ethyl benzene, etc. Traditionally, ethylene is mainly produced via naphtha cracking, whose prospect is greatly limited by the ever-decreasing petroleum resources, and its urgent production transmitting from petroleum to abundant gas-stuff, namely methane, is thus inevitable [1,2]. Over the past few decades, both direct and indirect routes to convert methane into olefins have been intensively explored. The indirect routes refer to methane reformings into syngas (with water, carbon dioxide, and/or oxygen), followed by syngas conversion into olefins via methanol or Fischer-Tropsch processes [3–5]. The direct ones include nonoxidative coupling of methane to olefins and aromatics [6–9] and oxidative coupling of methane (OCM) to C_2-C_3 hydrocarbons [10–15]. The indirect routes necessitate complicated processes as well as high equipment-energy costs, and the direct ones are hence desirable to be developed in spite of grand challenges. Moreover, in comparison with the nonoxidative coupling of methane, the appeal of OCM lies in its lower reaction temperature (usually 700–900 vs. 1000–1300 °C) [6–15].

The traditional OCM process co-feeds methane and gaseous oxygen into reactor with the presence of catalyst at around 800 °C. With gaseous oxygen co-fed, the as-formed C_2-C_3 products are prone to be deeply oxidized into CO and CO_2, thus resulting in the low C_2-C_3 selectivity. Besides, co-feeding methane with gaseous oxygen may lead to the potential safety hazards of CH_4-O_2 explosion, bringing great obstacles to the practical applications. Lastly, thermal effect of the co-feeding OCM reaction is of great challenge for managing the catalyst-bed temperature in a fixed bed reactor [16–19]. In principle, the OCM reaction via a chemical looping process (CL-OCM) is intrinsically safe since only the lattice oxygen in catalyst is utilized as oxidant rather than gaseous oxygen: CH_4 is fed into the fuel reactor and reacts with the oxidized-state catalyst to form C_2-C_3; subsequently, the as-reduced catalyst is oxidized by gaseous oxygen in the regenerator (Scheme S1) [20–24]. Therefore, the CL-OCM is an attractive alternative mode to the co-feeding OCM with several advantages. Particularly, the elimination of gaseous oxygen can avoid the deep oxidation of C_2-C_3 products, and the non-direct contacting of methane with oxygen can avoid the potential CH_4-O_2 explosion. Moreover, cost-intensive air separation process is not required because air can be directly used for catalyst regeneration (Scheme S1). Besides, the CL-OCM divides the heat of reaction into two reactors, which allows for the improved reaction-heat management [20].

* Corresponding author.
E-mail address: ylu@chem.ecnu.edu.cn (Y. Lu).

https://doi.org/10.1016/j.apcatb.2021.120948
Received 2 October 2021; Received in revised form 15 November 2021; Accepted 16 November 2021
Available online 23 November 2021
0926-3373/© 2021 Elsevier B.V. All rights reserved.

Despites these inherent advantages in CL mode, there still exist grand challenges in catalyst: first, the CH_4-converting lattice oxygen carrying capacity should be high enough, which is a guarantee for process efficiency (represented by product space time yield (STY), $g_{C2\text{-}C3}$ $kg_{cat.}^{-1}$ h^{-1}); second, this kind of lattice-oxygen species should be highly selective for converting CH_4 to C_2-C_3; last but not least, the catalyst should have good cyclic reaction-regeneration operation performance. Fang et al. [25] first reported the Mn_2O_3-Na_2WO_4/SiO_2 catalyst for co-feeding OCM process to perform a stable running for hundreds of hours. Consequently, Fleischer et al. [22] adopted it into CL-OCM process, reporting a maximum C_2 yield (CH_4 conversion times C_2 selectivity) of 25%; because CH_4-converting lattice oxygen carrying capacity of the Mn_2O_3-Na_2WO_4/SiO_2 is pretty low, the CL-OCM was performed at a very high catalyst/CH_4 weight ratio of 2793 thereby leading to an extremely low STY of 0.5 $g_{C2\text{-}C3}$ $kg_{cat.}^{-1}$ h^{-1}. Kustov et al. [26] reported an Ag-La_2O_3/SiO_2 catalyst, showing a high C_2 yield of 30% but using a very high catalyst/CH_4 weight ratio of 4050. Recently, He et al. [27] reported a Na-doped $LaMnO_3$ catalyst, achieving 30% CH_4 conversion with 55% C_2 selectivity but also using a high catalyst/CH_4 ratio of 1350 (STY of 0.8 $g_{C2\text{-}C3}$ $kg_{cat.}^{-1}$ h^{-1}). Undoubtedly, industrial application of above-mentioned catalysts in CL-OCM process is impossible due to unacceptably low process efficiency. Clearly, it is particularly desirable to render novel catalyst to substantially lower catalyst/CH_4 weight ratio to make CL-OCM process economical and practical. To accomplish this goal, Fan et al. [24] developed a Li-/W-decorated Mg_6MnO_8 catalyst, getting catalyst/CH_4 weight ratio dropped down to 135 while gaining and holding 28.6% C_2-C_3 yield (STY of 2.1 $g_{C2\text{-}C3}$ $kg_{cat.}^{-1}$ h^{-1}) within at least 100 cycles. Regardless of unacceptably low C_2-C_3 selectivity of 63.2% [24], great significance of this work lies in that decoration of oxygen storage material seem a strategy worth trying for catalyst design and tailoring toward efficient CL-OCM process. And, CL-OCM catalyst research should be focused on MnW-based system; on the one hand, supported Mn-W catalysts are active and selective in CH_4/O_2 co-feeding OCM reaction because of well-established synergistic catalysis [10,12,13,15], and on the other hand, Mn-containing oxygen storage materials (such as FeMn-based ones) not only have been extensively studied in chemical looping combustion [28,29] but also are not scarce.

Herein, we report the discovery of a promising Na_2WO_4/$FeMnO_3$ catalyst toward efficient CL-OCM process. The $FeMnO_3$ as oxygen carrier holds a high CH_4-converting lattice oxygen carrying capacity but favors combustion. Decoration of Na_2WO_4 mitigates the evolution of such CH_4-converting lattice oxygen stored in $FeMnO_3$ thereby getting the as-made catalyst working with highly selective conversion of CH_4 to C_2-C_3. The CL-OCM process using Na_2WO_4/$FeMnO_3$ catalyst is established by "$FeMnO_3 \leftrightarrow [MnFe_2O_4 + MnO]$" redox cycle, being capable of converting 20% CH_4 conversion into C_2-C_3 products with 80% selectivity at 800 °C and a short contacting time of 6 s, using a low catalyst/CH_4 weight ratio of 13.5. This catalyst achieves a high product STY of 29.8 $g_{C2\text{-}C3}$ $kg_{cat.}^{-1}$ h^{-1} and demonstrates good reaction-regeneration cycling performance within at least 50 cycles, showing a potential industrial CL-OCM implementation.

2. Experimental

2.1. Catalyst preparation

The Na_2WO_4/Mn_2O_3-Fe_2O_3 catalyst precursor with Na_2WO_4 loading of 6.9 wt% ($Na_2WO_4 \cdot 2H_2O$ as precursor) were obtained by the incipient wetness impregnation (IWI) method [10,13]. The Mn_2O_3 and Fe_2O_3 were first fully grinded in an agate mortar, and then the mixture was impregnated with 7 mL aqueous solution containing Na_2WO_4 (0.78 g, AR, Aladdin Industrial Co., Ltd.), followed by constant stirring for 1 h at room temperature to obtain the slurry, drying at 100 °C overnight and calcining at 800–1000 °C for 3 h in air to obtain catalysts. The catalysts obtained by calcining the Na_2WO_4/Mn_2O_3-Fe_2O_3 precursor (just dried after impregnation with Na_2WO_4) at 800, 900, 950 and 1000 °C are named as Na_2WO_4/$FeMnO_3$-800, Na_2WO_4/$FeMnO_3$-900, Na_2WO_4/-$FeMnO_3$-950 and Na_2WO_4/$FeMnO_3$-1000. The contrastive catalysts of Na_2WO_4/Mn_2O_3-SiC and Na_2WO_4/Fe_2O_3-SiC were prepared with same method except for replacing Fe_2O_3 or Mn_2O_3 with the same weight of SiC. The catalysts containing no Mn_2O_3 or Fe_2O_3 were synthesized by impregnating Fe_2O_3 or Mn_2O_3 with Na_2WO_4 aqueous solution and were named as Na_2WO_4/Fe_2O_3 and Na_2WO_4/Mn_2O_3. All catalysts were crushed and sieved to 100–120 meshes for catalysis evaluation.

2.2. Catalyst characterization

N_2 adsorption-desorption isotherms were measured at − 196 °C on a BELSORP-MAX (USA) gas adsorption analyzer after the catalysts were degassed under high vacuum at 300 °C for 6 h. The pore size distribution was determined by the Barrett-Joyner-Halenda (BJH) method. Powder X-ray diffraction (XRD) patterns were obtained on a Rigaku Ultra IV diffractometer (Japan), using Cu Kα radiation (λ = 0.1542 nm) at 40 kV and 30 mA in the 2θ scanning range of 10–90 ° at a scanning rate of 30 ° min^{-1}. The Raman measurements were carried out using a Raman spectrometer (Renishaw inVia) with a 532-nm semiconductor laser as excitation, equipped with a charge-coupled device camera enabling microanalysis on a sample point. The scanning range was set from 80 to 2000 cm^{-1}. The catalysts were characterized by scanning electron microscopy (SEM; Hitachi S-4800, Japan), transmission electron microscopy (TEM, FEI-Tecnai G2F30 spectrometer) equipped with an energy dispersive X-ray spectroscope (STEM-EDX).

H_2-TPR (H_2 temperature programmed reduction), O_2-TPD (O_2 temperature programmed desorption) and CH_4-TPSR (CH_4 temperature programmed surface reaction) were performed on TP5080 multifunctional automatic adsorption instrument (Xianquan Industrial and Trading Co., Ltd., China) with a thermal conductivity detector connected with a MS spectrometer (Proline Dycor, AMETEK Process Instrument, USA). The signals of different m/z were set to detect different products ($m/z = 28$ for CO and C_2H_4, $m/z = 44$ for CO_2, $m/z = 30$ for C_2H_6, $m/z = 27$ for C_2H_4 and C_2H_6, $m/z = 41$ for C_3H_6, $m/z = 32$ for O_2). For H_2-TPR experiments, catalyst of 0.1 g was first purified with 10 vol % O_2/Ar at 300 °C to remove the absorbed impurities on catalyst surface. After cooling down to room temperature in 10 vol% O_2/Ar, the gas was switched to H_2 and the temperature was elevated to 850 °C at 10 °C min^{-1} and held for 30 min at 850 °C. In each O_2-TPD or CH_4-TPSR experiment, 0.1 g catalyst was first purged with He (30 mL min^{-1}) at 300 °C for 30 min to remove the adsorbed impurities (such as CO_2, O_2 and/or H_2O) on catalyst surface. Thereafter, the catalyst bed was cooled to room temperature in He (30 mL min^{-1}). Then the temperature was elevated to 850 °C at 10 °C/min and held for 30 min at 850 °C in He (30 mL min^{-1}) for O_2-TPD and in CH_4 (30 mL min^{-1}) for CH_4-TPSR.

Thermogravimetric analysis (TGA, NET2SCH STA449F3) was applied to quantitatively determine the lattice-oxygen release rate. In detail, the catalysts were first purged with N_2 (20 mL min^{-1}) at 300 °C for 30 min to remove the adsorbed impurities (such as CO_2, O_2 and/or H_2O) on catalyst surface. Thereafter, the temperature was elevated to 800 °C in N_2 flow (20 mL min^{-1}). Once the temperature reached 800 °C, the gas flow was switched to 2 vol% CH_4/He (20 mL min^{-1}) for 10 min.

2.3. Reactivity tests

The CL-OCM experiments were carried out in a fixed bed quartz tube reactor (700 mm length with an internal diameter of 8 mm) that was placed in a split tubular furnace under atmospheric pressure. Catalyst of 1 g (about 1 mL) was sandwiched between 2 layers of quartz wool in the reactor. Two quartz sticks were placed below and above the quartz wool to reduce the dead volume of catalyst. Switching between methane and oxygen flows was employed during CL-OCM tests. The bed temperature was typically 800 °C and the samples were reduced by 10 mL min^{-1} methane for 10 min (the calculated weight ratio of catalyst to CH_4 is 13.5) at atmospheric pressure at reaction stage. The as-calculated

residence time was 6 s. The catalysts were then re-oxidized using oxygen (10 mL min^{-1}) for 5 min at regeneration stage. Between reaction and regeneration period, an inert gas purge (10 mL min^{-1} of Helium) of 2.5 min was inserted to prevent the mixing between methane and oxygen. One reaction-regeneration cycle was thus completed with twice Helium purging. During the reaction period, all of the exhausted gas (CH_4 and the purged gas of Helium were included) were collected in a gas sampling bag and then analyzed on an Agilent HP 6850 gas chromatography equipped with a TCD device, using a 30 m DM-Plot U capillary column (to separate CO_2, C_2H_4, C_2H_6, C_3H_6 and C_3H_8) and a 30 m DM-Plot molesieve capillary column (to separate O_2, N_2, CH_4 and CO) in parallel. The mean CH_4 conversion (C_{CH4}) and $C_2H_4/C_2H_6/C_3H_6/C_3H_8$ selectivity ($S_{C2\text{-}C3}$) were calculated using the standard normalization method on the basis of carbon atom balance and defined as follows (Eqs. 1, 2):

$$CH_4\ \text{conversion}\ (\%) = (2\times A_{C2H4}\times f_{C2H4}+2\times A_{C2H6}\times f_{C2H6}+3\times A_{C3H6}\times f_{C3H6}+3\times A_{C3H8}\times f_{C3H8}+A_{CO}\times f_{CO}+A_{CO2}\times f_{CO2})/(2\times A_{C2H4}\times f_{C2H4}+2\times A_{C2H6}\times f_{C2H6}+3\times A_{C3H6}\times f_{C3H6}+3\times A_{C3H8}\times f_{C3H8}+A_{CO}\times f_{CO}+A_{CO2}\times f_{CO2}+A_{CH4}\times f_{CH4})\times 100\% \quad (1)$$

$$C_2\text{-}C_3\ \text{selectivity}\ (\%) = (2\times A_{C2H4}\times f_{C2H4}+2\times A_{C2H6}\times f_{C2H6}+3\times A_{C3H6}\times f_{C3H6}+3\times A_{C3H8}\times f_{C3H8})/(2\times A_{C2H4}\times f_{C2H4}+2\times A_{C2H6}\times f_{C2H6}+3\times A_{C3H6}\times f_{C3H6}+3\times A_{C3H8}\times f_{C3H8}+A_{CO}\times f_{CO}+A_{CO2}\times f_{CO2})\times 100\% \quad (2)$$

where A_x is the peak area of component x in GC spectra of outlet gas and f_x is the relative molar correction factor (relative to C_6H_6) of component x (x = C_2H_4, C_2H_6, C_3H_6, C_3H_8, CO, CO_2, and CH_4).

Representing the gained weight of C_2-C_3 products over per gram catalyst per hour, space time yield (STY) was calculated as follows:

$$STY = V_{CH4,in}\times CH_4\ \text{conversion}\times\sum(C_y\ \text{selectivity}/y\times\rho_{Cy})/(W_{cat.}\times\text{redox time}) \quad (3)$$

where $V_{CH4,in}$ is the volume of CH_4 feed. C_y (C_2 or C_3) is the products containing y carbon atoms. ρ_{Cy} is the density of the products containing y carbon atoms at the conditions of atmospheric pressure, 25 °C. $W_{cat.}$ is the dosage of catalyst. Redox time is the overall time delay of one reaction-regeneration cycle (in the present study, the overall time delay of a cycle is 20 min, involving reaction time of 10 min, regeneration time of 5 min, and total helium purging time of 5 min, if not specified.).

3. Results and discussion

3.1. Catalyst precursor

The exploration was started by supporting 6.9 wt% Na_2WO_4 on a Mn_2O_3-Fe_2O_3 mixture with Mn_2O_3/Fe_2O_3 molar ratio of 1/1 to obtain Na_2WO_4/Mn_2O_3-Fe_2O_3 catalyst precursor. For comparison, two contrastive catalysts of Na_2WO_4/Mn_2O_3-SiC and Na_2WO_4/Fe_2O_3-SiC (with 6.9 wt% Na_2WO_4 loading) were also prepared by replacing Fe_2O_3 or Mn_2O_3 with the same mass of inert SiC, respectively. All catalysts were tested in multi-cycle CL-OCM process under optimized conditions: 800 °C, catalyst/CH_4 weight ratio of 13.5, CH_4 residence time of 6 s (Fig. S1 and supplementary text). As shown in Fig. 1 A, the Na_2WO_4/Mn_2O_3-Fe_2O_3 precursor becomes selective after undergoing an induction period. For each reaction-regeneration cycle, at 800 °C pure CH_4 flowed at 10 mL min^{-1} through the reactor with 1-gram catalyst for 10 min; the catalyst was then purged by Helium (10 mL min^{-1}) for 2.5 min, oxidized with O_2 (10 mL min^{-1}) for 5 min and purged by Helium (10 mL min^{-1}) for another 2.5 min before next cycle. Within the first 7 cycles, selectivity of C_2-C_3 rises gradually from 60% to 80% with a slight decline of CH_4 conversion from 23% to 20%. After that, both CH_4 conversion and C_2-C_3 selectivity remains unchanged within another 13 cycles. Similar performance evolution is also observed against cycle number over both Na_2WO_4/Mn_2O_3-SiC and Na_2WO_4/Fe_2O_3-SiC contrastive catalysts (Fig. S2). The Na_2WO_4/Fe_2O_3-SiC achieves very poor CH_4 conversion and C_2-C_3 selectivity of only 5% and 35%. Of interest is that 18.5% CH_4 conversion is obtainable with 60.5% selectivity to C_2-C_3 over Na_2WO_4/Mn_2O_3-SiC. The above results indicate that Mn_2O_3 can work synergistically with Na_2WO_4 in chemical looping mode while Fe_2O_3 shows paramount role in improving the synergistic catalysis between Mn_2O_3 and Na_2WO_4 in CL-OCM.

For comparison, our CL-OCM results in steady state as well as the reported ones (e.g., Mg_6MnO_8 [20], Li-Mg_6MnO_8 [23], (Li,W)-Mg_6MnO_8 [24], Ag-La_2O_3/SiO_2 [26], and Na-$LaMnO_3$ [27]) are summarized in Table S1. As can be seen, the reaction temperature for most catalysts is in the range of 800–850 °C. High CH_4 conversion of 30–50% could be obtained over the reported catalysts but with C_2-C_3 selectivity no more than 60%, e.g., 60% for Ag-La_2O_3/SiO_2 and 55% for Na-$LaMnO_3$. Especially, extremely high catalyst/CH_4 weight ratio (135–4050) is used, which is not industrially acceptable apparently. In contrast, high C_2-C_3 selectivity of 80% can be achieved in our case at an acceptable CH_4 conversion of 20% at 800 °C; most notably, catalyst/CH_4 weight ratio is substantially lowered down to 13.5, portending a high C_2-C_3 production capacity. Indeed, a high STY of 29.8 $g_{C2\text{-}C3}$ $kg_{cat.}^{-1}$ h^{-1} is achieved in this work, 15–60 times higher than those for the reported catalysts. Taking all factors (CH_4 conversion, C_2-C_3 selectivity, catalyst/CH_4 weight ratio, and C_2-C_3 production capacity) into consideration, our catalyst shows a substantial potential for industrial application.

3.2. Discovery of $Na_2WO_4/FeMnO_3$ catalyst

The Na_2WO_4/Mn_2O_3-Fe_2O_3 stands out from the samples but only after undergoing an induction period (Fig. 1A and Fig. S2), signifying the occurrence of chemical evolution and phase reconstruction that plays decisive role in improving the CL-OCM performance. To reach the essence, fresh and used Na_2WO_4/Mn_2O_3-Fe_2O_3 samples were initially probed by X-ray diffraction (XRD). As shown in Fig. 1B, the fresh one possesses distinguished XRD patterns of Mn_2O_3 and Fe_2O_3; after 10 reaction-regeneration cycles, however, perovskite $FeMnO_3$ is formed in association with disappearance of Fe_2O_3 and Mn_2O_3 (Fig. 1C). We also employed the Raman technique to confirm the $FeMnO_3$ formation. To unambiguously attribute the Raman bands to the components in our catalysts to be studied, the reference samples were first examined to obtain the reference Raman spectra (including $FeMnO_3$, Mn_2O_3, Fe_2O_3, MnO, $MnFe_2O_4$ and Mn_3O_4, Fig. S3). For the fresh Na_2WO_4/Mn_2O_3-Fe_2O_3, characteristic bands of Fe_2O_3 and Mn_2O_3 are detected (Fig. 1D). After 10 reaction-regeneration cycles, Raman bands of $FeMnO_3$ are exclusively observed, indicating the phase evolution from Fe_2O_3-Mn_2O_3 to $FeMnO_3$ (Fig. 1E), which is consistent with the XRD results (Fig. 1, B and C). The scanning electron microscope (SEM) images in Fig. S4 show clear growth of particles from 300 nm for the fresh catalyst precursor to 2.5 μm for the one after used with 10 cycles. Elemental mapping images in Fig. 1F visualizes obvious boundary between Mn and Fe for the fresh sample featured with Mn_2O_3-Fe_2O_3 mixture; in contrast, a homogeneous dispersion of Mn and Fe as well as W and Na elements is observed for the sample after used with 10 cycles (Fig. 1G). This indirectly confirms again the phase transformation from Fe_2O_3-Mn_2O_3 mixture to $FeMnO_3$. Clearly, fundamental shift of phase composition from Mn_2O_3-Fe_2O_3 mixture to a new $FeMnO_3$ compound is closely linked with the outstanding CL-OCM performance. Thus, the final catalyst is definitely identified to be $Na_2WO_4/FeMnO_3$, which works highly efficient and highly effective in CL-OCM reaction.

We firmly believe that this catalyst can be directly synthesized with no need of in-situ reaction treatment, according to the previous report that the $FeMnO_3$ can be formed by calcining Mn_2O_3-Fe_2O_3 mixture in air [30]. To check this idea, a series of catalyst samples were prepared by calcining the Na_2WO_4/Mn_2O_3-Fe_2O_3 precursor at 800, 900, 950, and 1000 °C for 3 h in air, named as $Na_2WO_4/FeMnO_3$-800, − 900, − 950, and − 1000, respectively. Their XRD phase evolution against the calcination temperature is shown in Fig. 2, A and B. With the calcination temperature elevated from 800 to 1000 °C, diffractions of $FeMnO_3$

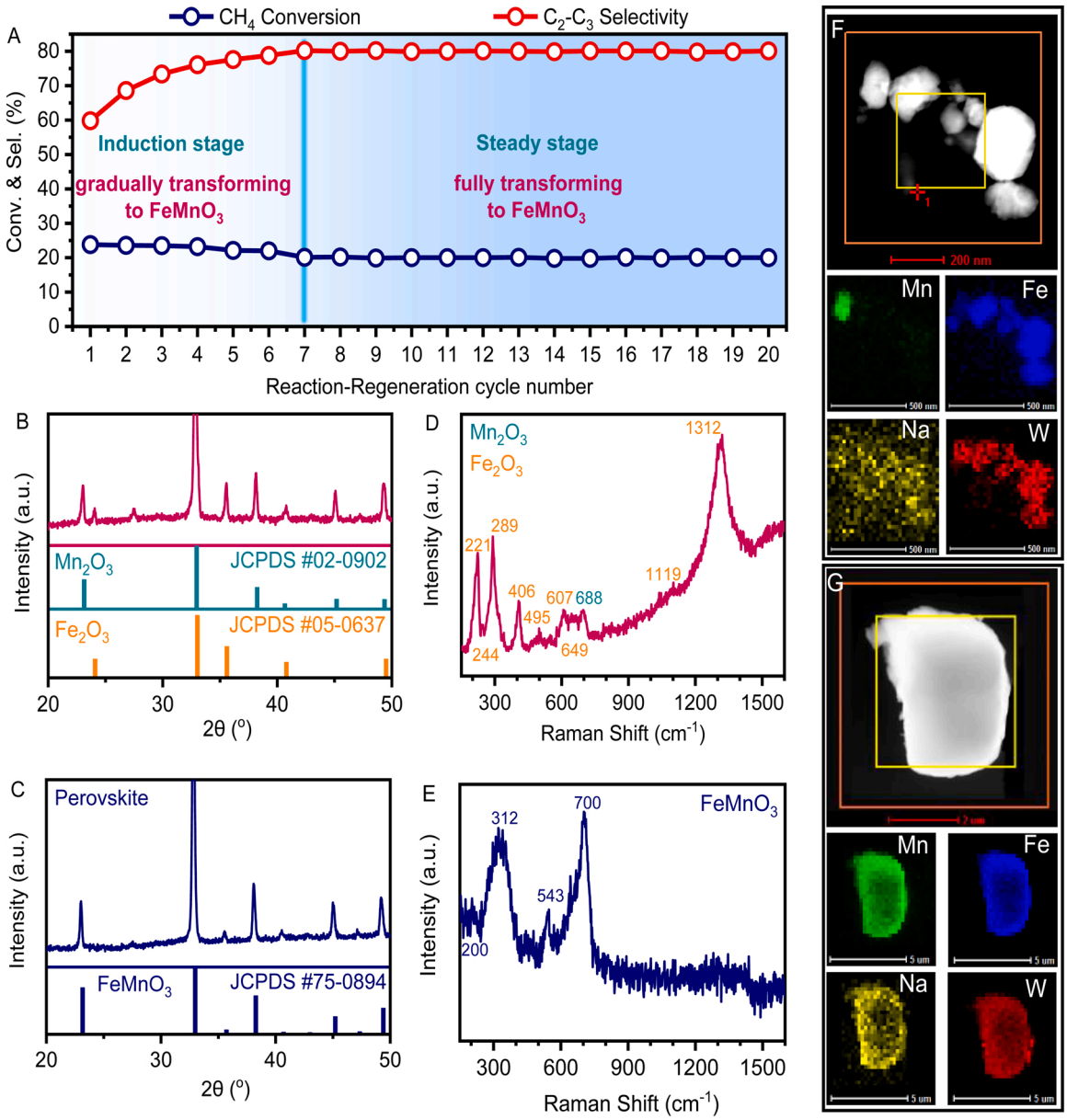

Fig. 1. The CL-OCM performance and chemical evolution of Na_2WO_4/Mn_2O_3-Fe_2O_3 catalyst precursor. (A) CH_4 conversion and C_2-C_3 selectivity over Na_2WO_4/Mn_2O_3-Fe_2O_3 precursor throughout 20 reaction-regeneration cycles. (B) XRD pattern, (D) Raman spectrum and (F) EDX maps of the freshly prepared Na_2WO_4/Mn_2O_3-Fe_2O_3 precursor. (C) XRD pattern, (E) Raman spectrum and (G) EDX maps of the re-oxidized Na_2WO_4/Mn_2O_3-Fe_2O_3 after 20 reaction-regeneration cycles. Reaction conditions: 800 °C, residence time of 6 s, catalyst/CH_4 weight ratio of 13.5. Regeneration conditions: 800 °C in O_2 flow for 5 min.

become stronger and sharper while the Fe_2O_3 and Mn_2O_3 diffractions weaken gradually until to disappearance at 1000 °C. A clear Na_2WO_4 phase is detected after calcining at and above 900 °C; a reasonable explanation is that phase transformation from Mn_2O_3-Fe_2O_3 mixture to $FeMn_2O_3$ markedly reduces the specific surface area of catalyst thereby leading to aggregation of Na_2WO_4. All these catalyst samples were tested in the CL-OCM reaction for 10 cycles. For the $Na_2WO_4/FeMnO_3$-800, − 900, and − 950, their CL-OCM reaction evolution is still characteristic of induction and steady stages (Fig. 2, C-E). Nevertheless, the induction period (i.e., fully transforming Mn_2O_3-Fe_2O_3 mixture to $FeMnO_3$; Fig. 1) is shortened to the fifth cycle for the $Na_2WO_4/FeMnO_3$-800 (Fig. 2C), fourth cycle for the $Na_2WO_4/FeMnO_3$-900 (Fig. 2D), while third cycle for the $Na_2WO_4/FeMnO_3$-950 (Fig. 2E). As expected but still excitingly, no induction stage is observed for the $Na_2WO_4/FeMnO_3$-1000 while achieving 80–82% C_2-C_3 selectivity and 18–20% CH_4 conversion from the start (Fig. 2F). Undoubtedly, formation of $FeMnO_3$ compounds is tightly linked with the markedly enhanced C_2-C_3 selectivity. We are confident that $FeMnO_3$ compounds work synergistically with Na_2WO_4 thereby enabling the CL-OCM reaction with high selectivity.

3.3. *Efficient CL-OCM established by "$FeMnO_3 \leftrightarrow [MnFe_2O_4 + MnO]$" redox cycle*

A question arises naturally: how does the $Na_2WO_4/FeMnO_3$ catalyst work to establish the chemical looping process? To seek an answer, the $Na_2WO_4/FeMnO_3$-1000 catalyst after reacting with CH_4 for 40 min at 800 °C was probed by XRD, showing that $FeMnO_3$ is reduced into $MnFe_2O_4$ (Fig. 3A). Notably, $FeMnO_3$ holds the Mn/Fe molar ratio of 1/1, whereas $MnFe_2O_4$ holds the ratio of 1/2. Since no Mn loses during the reaction-regeneration cycles, some other kind of Mn-containing

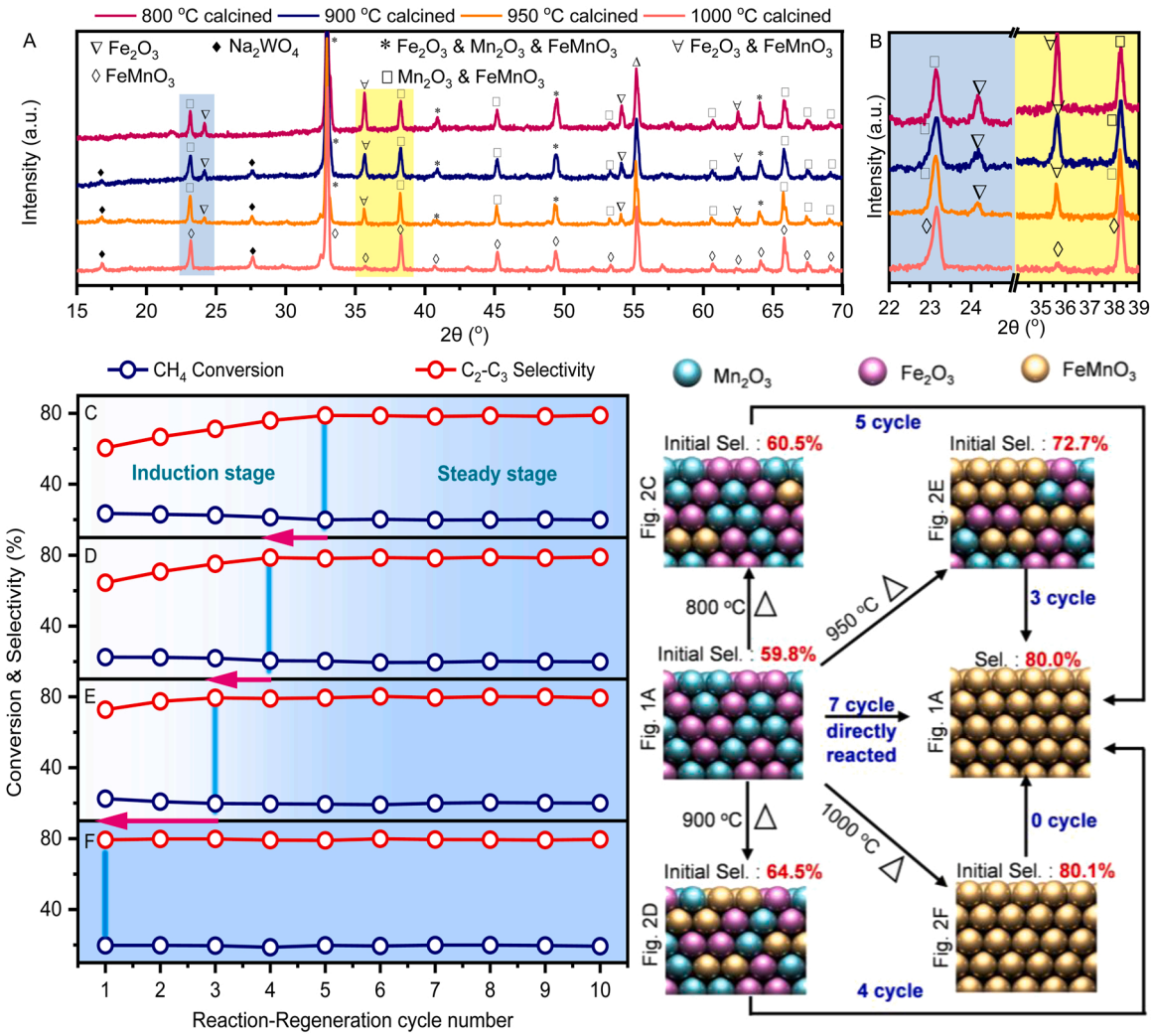

Fig. 2. Structural features and CL-OCM performance of $Na_2WO_4/FeMnO_3$ catalysts with varied calcination temperature. (A,B) Phase evolution of catalysts against calcination temperature from 800 to 1000 °C. CH_4 conversion and C_2-C_3 selectivity of $Na_2WO_4/FeMnO_3$ catalysts calcined at (C) 800 °C, (D) 900 °C, (E) 950 °C, and (F) 1000 °C.

compound accounting for the other 50% Mn may be formed, but is not detectable by XRD, undoubtedly due to its high dispersion. Indeed, MnO is really formed as evidenced by Raman at band of 1219 cm^{-1} in association with the formation of $MnFe_2O_4$ (with Raman bands at 321, 462, and 618 cm^{-1}) (Fig. 3B), revealing that OCM reaction proceeds via $FeMnO_3$ → [$MnFe_2O_4$ + MnO] reduction half-cycle. As-formed [$MnFe_2O_4$ + MnO] in OCM reaction can be easily transformed into $FeMnO_3$ again (i.e., the oxidation half-cycle; confirmed by XRD and Raman results in Fig. S5). We thus can draw a conclusion that CL-OCM catalysed by our $Na_2WO_4/FeMnO_3$ is established by "$FeMnO_3$ ↔ [$MnFe_2O_4$ + MnO]" redox cycle. To rule out the possibility that CL-OCM proceeds dominantly via either "Fe_2O_3 ↔ Fe_3O_4" or "Mn_2O_3 ↔ [Mn_3O_4 + MnO]" redox cycle, two Na_2WO_4/Fe_2O_3 and Na_2WO_4/Mn_2O_3 (with 6.9 wt% Na_2WO_4 loading) contrastive catalysts were prepared and tested in this reaction process. For the Na_2WO_4/Fe_2O_3, minute quantity of Fe_2O_3 is reduced into Fe_3O_4 after reacting with CH_4 at 800 °C for 10 min while delivering a CH_4 conversion of only 7%, indicating very low CH_4-converting lattice-oxygen carrying capacity (Fig. 3, C and D). For the Na_2WO_4/Mn_2O_3, Mn_2O_3 is reduced into [Mn_3O_4 + MnO] while [Mn_3O_4 + MnO] can be circulated into Mn_2O_3, establishing a "Mn_2O_3 ↔ [Mn_3O_4 + MnO]" redox cycle (Fig. 3, E and F). This catalyst offers 28% CH_4 conversion but a very low C_2-C_3 selectivity of 58%. Given that in the "$FeMnO_3$ ↔ [$MnFe_2O_4$ + MnO]" redox cycle, only the valence state of Mn is reciprocated with Fe remaining constant, the cleavage of Mn-O bond is responsible for releasing lattice-oxygen to convert CH_4, which is similar with the report by Gong et al. [31]. In addition, the Na_2WO_4/Fe_2O_3 gives very low CH_4 conversion, because Fe_2O_3 holds a thimbleful of useable lattice oxygen under our CL-OCM reaction conditions (Fig. 3, C and D). Accordingly, we infer that CH_4 conversion will drop with C_2-C_3 selectivity almost unchanged if reducing $FeMnO_3$ content in catalyst. To check this inference, another contrastive catalyst was prepared by calcining a Na_2WO_4/Mn_2O_3-Fe_2O_3 precursor with Mn_2O_3/Fe_2O_3 molar ratio of 3/7 (Fe_2O_3-rich) at 1000 °C and was examined in CL-OCM. As expected, this catalyst achieves a C_2-C_3 selectivity (81%) comparable to that (80%) for the Na_2WO_4/-$FeMnO_3$-1000 but a lower CH_4 conversion of 15% (Fig. S6). The above control experimental results unanimously confirm again that our $Na_2WO_4/FeMnO_3$ catalyst works primarily through "$FeMnO_3$ ↔ [$MnFe_2O_4$ + MnO]" redox cycle toward efficient CL-OCM especially with markedly enhanced selectivity.

3.4. *Lattice-oxygen evolution tuned by "$FeMnO_3$ → [$MnFe_2O_4$ + MnO]"*

Despite above exciting advances, why such "$FeMnO_3$ ↔ [$MnFe_2O_4$ + MnO]" redox cycle plays essential role in improving catalyst selectivity (Set aside for a moment the contribution of Na_2WO_4) still remains

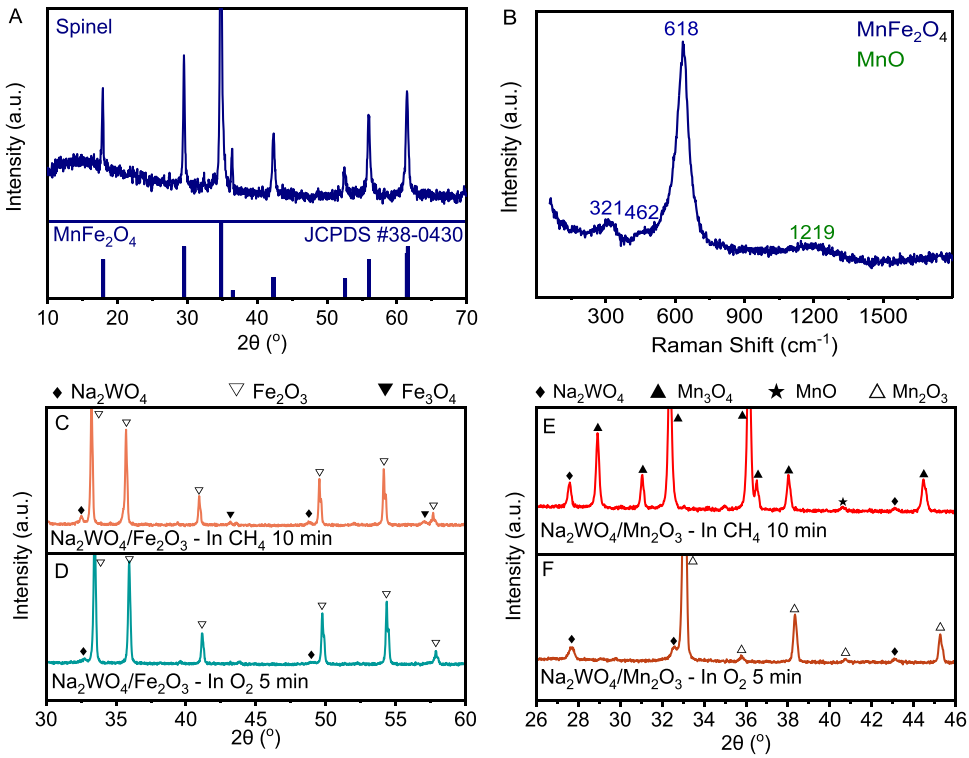

Fig. 3. Phase evolution of catalysts. (A) XRD pattern and (B) Raman spectrum of $Na_2WO_4/FeMnO_3$-1000 catalyst after reacting with CH_4 for 40 min. XRD patterns of the Na_2WO_4/Fe_2O_3 catalyst after (C) 10-minute CH_4 reduction and (D) 5-minute O_2 oxidation. XRD patterns of the Na_2WO_4/Mn_2O_3 catalyst after (E) 10-minute CH_4 reduction and (F) 5-minute O_2 oxidation.

to be unveiled, in comparison with the "$Mn_2O_3 \leftrightarrow [Mn_3O_4 + MnO]$" redox cycle also established in Na_2WO_4/Mn_2O_3. Some studies reported that the release of lattice oxygen should be elaborately controlled to prevent the over-oxidation of C_2-C_3 products [20]. We speculate that selectivity-relevant lattice-oxygen release is tuned by "$FeMnO_3 \rightarrow [MnFe_2O_4 + MnO]$" half cycle to a great extent. To prove this point, lattice-oxygen release of the $Na_2WO_4/FeMnO_3$ catalysts calcined at 800–1000 °C was investigated by using hydrogen-temperature programmed reduction (H_2-TPR) method, which can effectively distinguish the lattice-oxygen evolution activity. In Fig. S7, H_2-TPR profiles are recorded for all the catalysts as well as Na_2WO_4/Mn_2O_3 and Na_2WO_4/Fe_2O_3 for reference. The Na_2WO_4/Mn_2O_3 offers two H_2-consumption peaks at 475 and 700 °C, attributed to Mn_2O_3-to-Mn_3O_4 and Mn_3O_4-to-MnO, respectively (Fig. S7A) [32,33], while the Na_2WO_4/Fe_2O_3 shows a triple-peak profile consisting of Fe_2O_3-to-Fe_3O_4 at 500–600 °C, Fe_3O_4-to-FeO at 690–700 °C, and FeO-to-Fe^0 at 850 °C (Fig. S7B) [34,35]. The Na_2WO_4/Mn_2O_3-Fe_2O_3 precursor delivers a H_2-TPR profile very close to the sum of profiles of Na_2WO_4/Mn_2O_3 and Na_2WO_4/Fe_2O_3, with climax peaked at 710 °C (Fig. S7C). For the $Na_2WO_4/FeMnO_3$ catalysts, the H_2-consumption amounts below 700 °C are gradually reduced with catalyst calcination temperature rising from 800 to 1000 °C, while leading to the shifting of main H_2-consumption peak from 745 to 762 °C. By combining this information with the fact of facilitated transformation of Fe_2O_3-Mn_2O_3 mixture into $FeMnO_3$ with elevating calcination temperature (Fig. 2, A and B), we believe that the formation of $FeMnO_3$ exerts dual effects: (1) cleaning up easily reducible lattice-oxygen species (from free Fe_2O_3 and Mn_2O_3 species); (2) moderately reducing the reducibility of Mn-O bond (reduction temperature increased by 60 °C) while preventing Fe^{3+} from reduction.

Moreover, CH_4-temperature programmed surface reaction combined with mass-spectrometry (CH_4-TPSR-MS) experiments were conducted to probe the reactivity of different lattice-oxygen species. Fig. S8 displays the CH_4-TPSR-MS profiles of a series of $Na_2WO_4/FeMnO_3$ catalysts after calcining at 800–1000 °C. Over the Na_2WO_4/Fe_2O_3-Mn_2O_3 precursor (as reference), only CO_2 signal with moderate intensity is detected at 350–600 °C (Fig. S8A) due to the catalytic combustion of CH_4 at surfaces of free Mn_2O_3 and Fe_2O_3 individuals; signals of C_2H_4, C_2H_6, C_3H_6, and CO as well as O_2 emerge from 600 °C and all are peaked at 760 °C (Fig. S8A). By comparison, over the $Na_2WO_4/FeMnO_3$ catalysts CO_2 signal intensity at 350–600 °C markedly weakens with catalyst calcination temperature elevated (Fig. S8, B to E). The signal peak temperature relevant to OCM reaction shifts from 760 °C for the Na_2WO_4/Fe_2O_3-Mn_2O_3 precursor gradually to 840 °C for the $Na_2WO_4/FeMnO_3$-1000 catalyst (Fig. S8F). Moreover, the calcined catalysts all achieve much stronger C_2-C_3 product signals than the Na_2WO_4/Fe_2O_3-Mn_2O_3 precursor. Most notably, formation of C_2-C_3 products is accompanied by O_2 desorption, indicating that OCM reaction taken place is tightly linked with lattice-oxygen release while the selectivity is subject to lattice-oxygen activity (i.e., more $FeMnO_3$ is formed, lower the lattice-oxygen activity but higher the C_2-C_3 selectivity; Fig. 2, Fig. 3, and Fig. S8).

We initially explore the lattice-oxygen evolution by measuring the reduction rate of Mn^{3+} (corresponding to Mn_2O_3 and/or $FeMnO_3$) using XRD to monitor the time-dependent phase change of the catalysts exposed in CH_4 flow at 800 °C, with the results shown in Fig. S9. For all catalysts, the Mn^{3+} can be fully reduced into Mn^{2+} (corresponding to Mn_2O_3 and/or $FeMnO_3$ reduced into $MnFe_2O_4$ and MnO) in CH_4 flow but with different reduction rate (represented by time length needed to reach full reduction): 9 min for the Na_2WO_4/Fe_2O_3-Mn_2O_3 precursor, 13 min for the one calcined at 800 °C, 15 min for at 900 °C, 27 min for at 950 °C, and 35 min for at 1000 °C (Fig. 4A). The ever-prolonged time length for Mn^{3+} reduction indicates the ever-lowered lattice-oxygen activity, which is in line with the ever-increased formation of $FeMnO_3$ with catalyst calcination temperature. The oxygen-temperature programmed desorption combined with mass-spectrometry (O_2-TPD-MS)

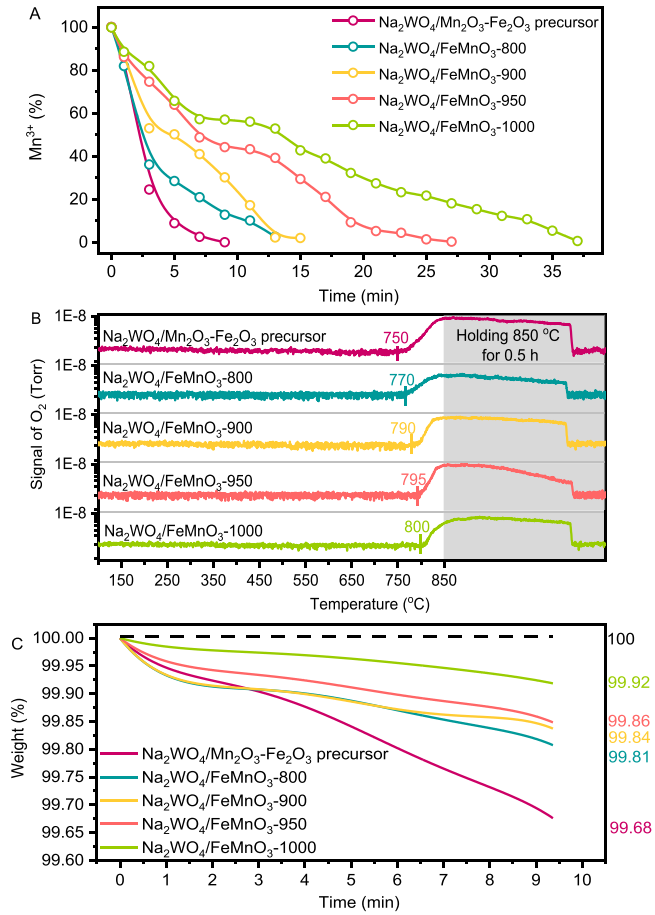

Fig. 4. Lattice-oxygen activity of the Na_2WO_4/Mn_2O_3-Fe_2O_3 catalyst precursor and the $Na_2WO_4/FeMnO_3$ catalysts with varied calcination temperature from 800 to 1000 °C. (A) Calculated Mn^{3+} fraction based on XRD patterns. (B) Signals of $m/z = 32$ in O_2-TPD-MS profiles. (C) TG analyses at 800 °C in 2 vol% CH_4/He for 10 min.

experiments were also conducted to understand the $FeMnO_3$-governed lattice-oxygen evolution, with the results shown in Fig. 4B. As we can see, all catalysts have comparable amount of desorptive lattice oxygen carrying capacity evidenced by their close O_2-signal intensity, whereas the onset temperature of lattice-oxygen desorption shows an obvious movement towards higher temperature with the catalyst calcination temperature. Such backward movement of lattice-oxygen desorption validates again the lowered lattice-oxygen activity in company with the $FeMnO_3$ formation. The lattice-oxygen release rate was quantitatively determined by thermal gravity analyses (TGA) accordingly [31]. As shown in Fig. 4C, in 2 vol% CH_4/He flow at 800 °C for 10 min, the Na_2WO_4/Mn_2O_3-Fe_2O_3 precursor offers the highest weight loss of 0.32 wt% while the weight loss of the catalysts is gradually reduced against their calcination temperature from 800 to 1000 °C. Particularly, the $Na_2WO_4/FeMnO_3$-1000 shows the lowest loss of only 0.08 wt% within 10 min. The lattice-oxygen release rate (μmol[O] $g_{cat.}^{-1}$ h^{-1}) for these catalysts deduced from TGA data is displayed in Table S2, showing an order: 1200 for Na_2WO_4/Mn_2O_3-Fe_2O_3 catalyst precursor > 712.5 for $Na_2WO_4/FeMnO_3$-800 > 600 for $Na_2WO_4/FeMnO_3$-900 > 525 for $Na_2WO_4/FeMnO_3$-950 > 300 for $Na_2WO_4/FeMnO_3$-1000. By combining this information with the facts of ever-increasing $FeMnO_3$ formation with calcination temperature rising (Fig. 2, A and B) and efficient CL-OCM established by "$FeMnO_3 \leftrightarrow [MnFe_2O_4 + MnO]$" redox cycle, the $FeMnO_3$ is paramount for the marked improvement of C_2-C_3 selectivity, in nature due to substantially lowered lattice-oxygen release rate via "$FeMnO_3$ to $[MnFe_2O_4 + MnO]$" (Fig. 4) in the presence of Na_2WO_4 thereby suppressing the over-oxidation.

3.5. Na_2WO_4 slowing lattice-oxygen release from $FeMnO_3$

Whereas the "$FeMnO_3 \leftrightarrow [MnFe_2O_4 + MnO]$" redox cycle plays the most fundamental role in getting the $Na_2WO_4/FeMnO_3$ catalyst running efficiently in the CL-OCM process, it is still unclear what role Na_2WO_4 plays in this catalyst system. To seek an answer, $FeMnO_3$ (obtained by calcining Mn_2O_3-Fe_2O_3 at 1000 °C in air, Fig. S10A) were prepared and its reduction weight loss in 2 vol% CH_4/He flow at 800 °C for 10 min was monitored by TGA. As shown in Fig. S10A, $FeMnO_3$ delivers a lattice-oxygen consumption rate of 1987.5 μmol[O] $g_{cat.}^{-1}$ h^{-1} (calculated based on weight loss of 0.53 wt% within 10 min), and offers a low C_2-C_3 selectivity of 15.5% (Fig. S10B). Interestingly, adding 6.9 wt% Na_2WO_4 onto $FeMnO_3$ (i.e., the $Na_2WO_4/FeMnO_3$ catalyst) makes the lattice-oxygen consumption rate decreased by a factor of 6.6 (i.e., 300 μmol[O] $g_{cat.}^{-1}$ h^{-1}; Fig. 4C and Fig. S10A), and the C_2-C_3 selectivity correspondingly increases to 80–82% (Fig. 2F). Formation of a core-shell-like $FeMnO_3$@Na_2WO_4 structure is observed by high-resolution transmission electron microscope (HRTEM, Fig. 5), which might account for slowing lattice-oxygen release from $FeMnO_3$. As previously explored for the oxidative dehydrogenation of ethane via a cyclic redox scheme by Li et al. [36], Li_2CO_3 or Na_2WO_4 physically covers the Mn-based oxides to not only block the non-selective sites on oxides surfaces but also offer the transmission medium for oxygen species with a controllable rate, which is a possible explanation.

3.6. Testing scale-up

The above results and analyses represent that the $Na_2WO_4/FeMnO_3$ catalyst is a qualified catalyst toward efficient CL-OCM process (C_2-C_3 selectivity of 80%, C_2-C_3 production capacity of 29.8 $g_{C2\text{-}C3}$ $kg_{cat.}^{-1}$ h^{-1}, and particularly stability) (Fig. 1A, and Fig. S11). We wonder whether such performance could be sustained if the $Na_2WO_4/FeMnO_3$ catalyst is adopted in a larger scale process. We scaled up the CL-OCM testing by increasing the dosage of $Na_2WO_4/FeMnO_3$-1000 catalyst from 1 to 10 g (loaded into a quartz tubular reactor of 400 mm length and 25 mm internal diameter), with reaction conditions remaining identical (i.e., residence time of 6 s and catalyst/CH_4 weight ratio of 13.5). As can be seen in Fig. S12, with reaction temperature rising from 780 to 800 °C, CH_4 conversion is increased from 16.5% to 20% with a slight reduction of C_2-C_3 selectivity from 83% to 79%, while the olefin/paraffin ratio is increased from 2.2 to 3.0. Scale-up of CL-OCM testing with 10-gram catalyst also yields comparable results seen in the case of using 1-gram catalyst (Fig. 1A and Fig. S12), showing substantial application potential of the $Na_2WO_4/FeMnO_3$ catalyst in practical CL-OCM process.

4. Conclusions

The OCM reaction via a chemical looping process (CL-OCM) is an attractive alternative mode to the co-feeding OCM process with several advantages such as intrinsic safety, easy heat management, and substantial potential for improving the selectivity. Commercial exploitation of the CL-OCM process is urgently calling for a qualified catalyst with high carrying capacity of selective CH_4-converting lattice oxygen, which is a guarantee of an acceptable process efficiency in the real practice but

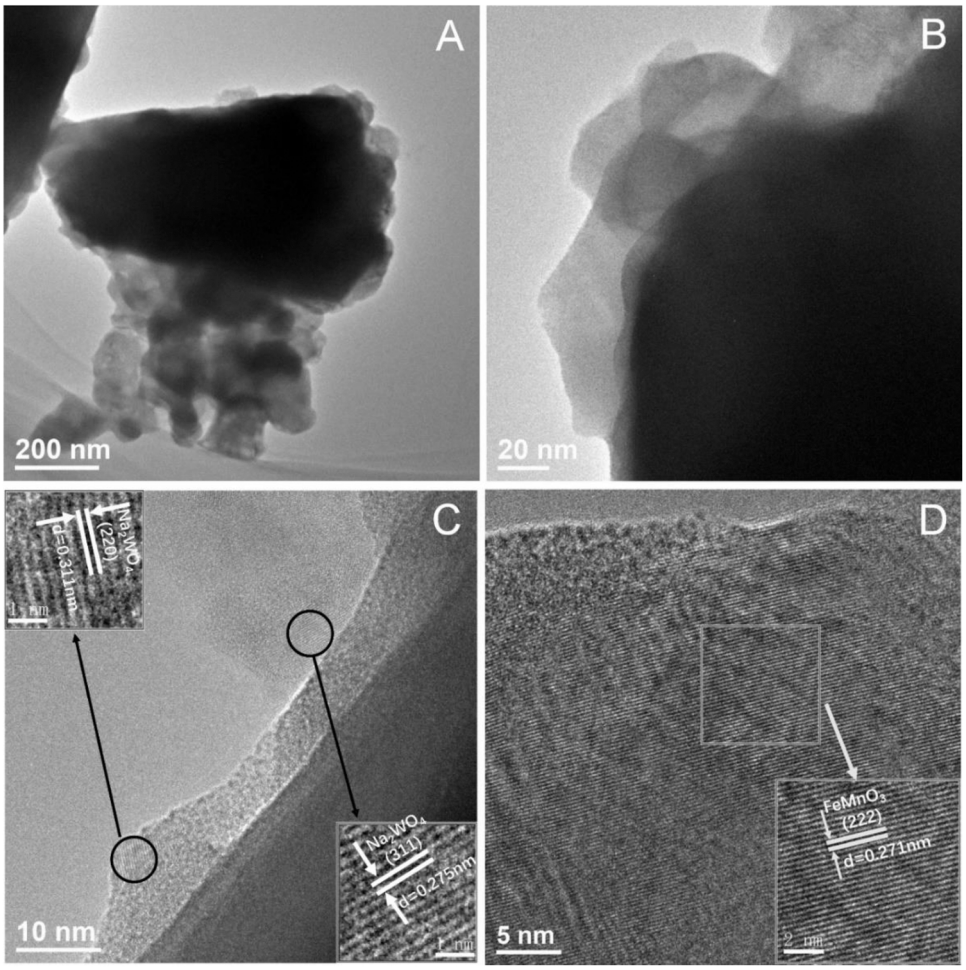

Fig. 5. Core-shell-like structure of the $Na_2WO_4/FeMnO_3$-1000 catalyst. (A-D) HRTEM images of used $Na_2WO_4/FeMnO_3$-1000 catalyst ending in oxidative state.

is a challenging area. In this context, decoration of oxygen storage material seems a strategy worth trying for design and tailoring of a high-performance CL-OCM catalyst. Along this line of thinking, a promising $Na_2WO_4/FeMnO_3$ catalyst is developed via directly calcining a Na_2WO_4-decorated mixture of Mn_2O_3 and Fe_2O_3 at 1000 °C in air. This catalyst is working effectively and efficiently via the redox cycle of $FeMnO_3 \leftrightarrow [MnFe_2O_4 + MnO]$ with good cycling performance, achieving a high target product STY of 29.8 $g_{C2\text{-}C3}$ $kg_{cat.}^{-1}$ h^{-1} with 20% CH_4 conversion and 80% C_2-C_3 selectivity at 800 °C and a low catalyst/CH_4 weight ratio of 13.5. In comparison with the literature catalysts, our catalyst increases the CL-OCM process efficiency (expressed as STY) by 15–60 times while leading to hundreds of times reduction of the catalyst/CH_4 weight ratio. Decoration of Na_2WO_4 mitigates the evolution of such CH_4-converting lattice oxygen stored in $FeMnO_3$ thereby getting the as-made catalyst worked with highly selective conversion of CH_4 to C_2-C_3. Moreover, scale-up of CL-OCM testing is also successfully performed with good maintenance of CH_4 conversion and C_2-C_3 selectivity with high productivity, validating its promising potential in practical application. We are confident that our findings will stimulate attempts to render more advanced CL-OCM catalysts through finely tuning of oxygen storage materials.

Funding

This work was supported by the National Natural Science Foundation of China (22072043, 21773069, 21703069), and a Key Basic Research Project (18JC1412100) from the Shanghai Municipal Science and Technology Commission.

CRediT authorship contribution statement

Y. Lu conceived the idea for the project and directed the research. W. S., Y.G., and J.S. conducted material synthesis, and performed structural characterizations and catalytic test. W.S., G.Z., and Y. Liu analyzed the catalytic results. W.S., G.Z. and Y. Lu drafted the manuscript. All authors discussed and commented on the manuscript. W.S. and G.Z. are contributed equally.

Declaration of Competing Interest

The authors declare that they have no known competing financial interests or personal relationships that could have appeared to influence the work reported in this paper.

Y. Lu, W.S., G.Z. J.S. and Y. Liu have a patent application related to this work filed with the Chinese Patent Office on 16 March 2020 (202010180696.6).

Data Availability

All data needed to evaluate the conclusions in the paper are present in the paper and/or the Supplementary Materials.

Acknowledgments

None.

Appendix A. Supporting information

Supplementary data associated with this article can be found in the online version at doi:10.1016/j.apcatb.2021.120948.

References

[1] T. Ren, M. Patel, K. Blok, Steam cracking and methane to olefins: energy use, CO_2 emissions and production costs, Energy 33 (2008) 817–833.

[2] V.S. Arutyunov, L.N. Strekova, The interplay of catalytic and gas-phase stages at oxidative conversion of methane: a review, J. Mol. Catal. A Chem. 426 (2017) 326–342.

[3] J.M. Fox, The different catalytic routes for methane valorization: an assessment of processes for liquid fuels, Catal. Rev. 35 (1993) 169–212.

[4] F. Jiao, J. Li, X. Pan, J. Xiao, H. Li, H. Ma, M. Wei, Y. Pan, Z. Zhou, M. Li, S. Miao, J. Li, Y. Zhu, D. Xiao, T. He, J. Yang, F. Qi, Q. Fu, X. Bao, Selective conversion of syngas to light olefins, Science 351 (2016) 1065–1068.

[5] L. Zhong, F. Yu, Y. An, Y. Zhao, Y. Sun, Z. Li, T. Lin, Y. Lin, X. Qi, Y. Dai, L. Gu, J. Hu, S. Jin, Q. Shen, H. Wang, Cobalt carbide nanoprisms for direct production of lower olefins from syngas, Nature 538 (2016) 84–87.

[6] I. Vollmer, S. Ould-Chikh, A. Aguilar-Tapia, G. Li, E. Pidko, J.L. Hazemann, F. Kapteijn, J. Gascon, Activity descriptors derived from comparison of Mo and Fe as active metal for methane conversion to aromatics, J. Am. Chem. Soc. 141 (2019) 18814–18824.

[7] X. Guo, G. Fang, G. Li, H. Ma, H. Fan, L. Yu, C. Ma, X. Wu, D. Deng, M. Wei, D. Tan, R. Si, S. Zhang, J. Li, L. Sun, Z. Tang, X. Pan, X. Bao, Direct, nonoxidative conversion of methane to ethylene, aromatics, and hydrogen, Science 344 (2014) 616–619.

[8] A.L. Dipu, S. Ohbuchi, Y. Nishikawa, S. Iguchi, H. Ogihara, I. Yamanaka, Direct nonoxidative conversion of methane to higher hydrocarbons over Silica-supported nickel phosphide catalyst, ACS Catal. 10 (2019) 375–379.

[9] S.C. Oh, E. Schulman, J. Zhang, J. Fan, Y. Pan, J. Meng, D. Liu, Direct non-oxidative methane conversion in a millisecond catalytic wall reactor, Angew. Chem. Int. Ed. 58 (2019) 7083–7086.

[10] P. Wang, G. Zhao, Y. Wang, Y. Lu, $MnTiO_3$-driven low-temperature oxidative coupling of methane over TiO_2-doped Mn_2O_3-Na_2WO_4/SiO_2 catalyst, Sci. Adv. 3 (2017), e1603180.

[11] T. Ito, J.H. Lunsford, Synthesis of ethylene and ethane by partial oxidation of methane over lithium-doped magnesium oxide, Nature 314 (1985) 721–722.

[12] N.S. Hayek, G.J. Khlief, F. Horani, O.M. Gazit, Effect of reaction conditions on the oxidative coupling of methane over doped MnO_x-Na_2WO_4/SiO_2 catalyst, J. Catal. 376 (2019) 25–31.

[13] S. Arndt, T. Otremba, U. Simon, M. Yildiz, H. Schubert, R. Schomäcker, Mn-Na_2WO_4/SiO_2 as catalyst for the oxidative coupling of methane. What is really known? Appl. Catal. A Gen. 425 (2012) 53–61.

[14] M. Sinev, E. Ponomareva, I. Sinev, V. Lomonosov, Y. Gordienko, Z. Fattakhova, D. Shashkin, Oxygen pathways in oxidative coupling of methane and related processes. Case study: NaWMn/SiO_2 catalyst, Catal. Today 333 (2019) 36–46.

[15] Z. Aydin, V.A. Kondratenko, H. Lund, S. Bartling, C.R. Kreyenschulte, D. Linke, E. V. Kondratenko, Revisiting activity- and selectivity-enhancing effects of water in the oxidative coupling of methane over MnO_x-Na_2WO_4/SiO_2 and proving for other materials, ACS Catal. 10 (2020) 8751–8764.

[16] S. Pak, J.H. Lunsford, Thermal effects during the oxidative coupling of methane over Mn/Na_2WO_4/SiO_2 and Mn/Na_2WO_4/MgO catalysts, Appl. Catal. A Gen. 168 (1998) 131–137.

[17] S. Sarsani, D. West, W. Liang, V. Balakotaiah, Autothermal oxidative coupling of methane with ambient feed temperature, Chem. Eng. J. 328 (2017) 484–496.

[18] B. Zohour, D. Noon, S. Senkan, New insights into the oxidative coupling of methane from spatially resolved concentration and temperature profiles, ChemCatChem 5 (2013) 2809–2812.

[19] V. Balakotaiah, D.H. West, Thermal effects and bifurcations in gas phase catalytic partial oxidations, Curr. Opin. Chem. Eng. 5 (2014) 68–77.

[20] E.Y. Chung, W.K. Wang, S.G. Nadgouda, D.S. Baser, J.A. Sofranko, L.-S. Fan, Catalytic oxygen carriers and process systems for oxidative coupling of methane using the chemical looping technology, Ind. Eng. Chem. Res. 55 (2016) 12750–12764.

[21] S. Parishan, P. Littlewood, A. Arinchtein, V. Fleischer, R. Schomäcker, Chemical looping as a reactor concept for the oxidative coupling of methane over the Mn_xO_y-Na_2WO_4/SiO_2 catalyst, benefits and limitation, Catal. Today 311 (2018) 40–47.

[22] V. Fleischer, P. Littlewood, S. Parishan, R. Schomäcker, Chemical looping as reactor concept for the oxidative coupling of methane over a Na_2WO_4/Mn/SiO_2 catalyst, Chem. Eng. J. 306 (2016) 646–654.

[23] Z. Cheng, D.S. Baser, S.G. Nadgouda, L. Qin, J.A. Fan, L.-S. Fan, C_2 selectivity enhancement in chemical looping oxidative coupling of methane over a Mg-Mn composite oxygen carrier by Li-doping-induced oxygen vacancies, ACS Energy Lett. 3 (2018) 1730–1736.

[24] D.S. Baser, Z. Cheng, J.A. Fan, L.-S. Fan, Codoping Mg-Mn based oxygen carrier with lithium and tungsten for enhanced C_2 yield in a chemical looping oxidative coupling of methane system, ACS Sustain. Chem. Eng. 9 (2021) 2651–2660.

[25] X. Fang, S. Li, J. Lin, J. Gu, D. Yan, Preparation and characterization of catalyst for oxidative coupling of methane, J. Mol. Catal. 6 (1992) 254–262.

[26] J.S. Sung, K.Y. Choo, T.H. Kim, A. Greish, L. Glukhov, E. Finashina, L. Kustov, Peculiarities of oxidative coupling of methane in redox cyclic mode over Ag-La_2O_3/SiO_2 catalysts, Appl. Catal. A Gen. 380 (2010) 28–32.

[27] S. Jiang, W. Ding, K. Zhao, Z. Huang, G. Wei, Y. Feng, Y. Lv, F. He, Enhanced chemical looping oxidative coupling of methane by Na-doped $LaMnO_3$ redox catalysts, Fuel 299 (2021), 120932.

[28] R. Pérez-Vega, A. Abad, M.T. Izquierdo, P. Gayán, L.F. de Diego, J. Adánez, Evaluation of Mn-Fe mixed oxide doped with TiO_2 for the combustion with CO_2 capture by chemical looping assisted by oxygen uncoupling, Appl. Energy 237 (2019) 822–835.

[29] A. Abad, R. Pérez-Vega, L.F. de Diego, P. Gayán, M.T. Izquierdo, F. García-Labiano, J. Adánez, Thermochemical assessment of chemical looping assisted by oxygen uncoupling with a MnFe-based oxygen carrier, Appl. Energy 251 (2019), 113340.

[30] C. Doroftei, P.D. Popa, E. Rezlescu, N. Rezlescu, Structural and catalytic characterization of nanostructured iron manganite, Compos. B Eng. 67 (2014) 179–182.

[31] S. Chen, L. Zeng, R. Mu, C. Xiong, Z. Zhao, C. Zhao, C. Pei, L. Peng, J. Luo, L.S. Fan, J. Gong, Modulating lattice-oxygen in dual-functional Mo-V-O mixed oxides for chemical looping oxidative dehydrogenation, J. Am. Chem. Soc. 141 (2019) 18653–18657.

[32] X. Zhang, H. Li, F. Hou, Y. Yang, H. Dong, N. Liu, Y. Wang, L. Cui, Synthesis of highly efficient Mn_2O_3 catalysts for CO oxidation derived from Mn-MIL-100, Appl. Surf. Sci. 411 (2017) 27–33.

[33] H. Jiang, C. Wang, H. Wang, M. Zhang, Synthesis of highly efficient MnO_x catalyst for low-temperature NH_3-SCR prepared from Mn-MOF-74 template, Mater. Lett. 168 (2016) 17–19.

[34] M. Liang, W. Kang, K. Xie, Comparison of reduction behavior of Fe_2O_3, ZnO and $ZnFe_2O_4$ by TPR technique, J. Nat. Gas. Chem. 18 (2009) 110–113.

[35] D. Cui, M. Li, Y. Qiu, L. Ma, D. Zeng, R. Xiao, Improved hydrogen production with 100% fuel conversion through the redox cycle of $ZnFeAlO_x$ oxygen carrier in chemical looping scheme, Chem. Eng. J. 400 (2020).

[36] Y. Gao, X. Wang, J. Liu, C. Huang, K. Zhao, Z. Zhao, X. Wang, F. Li, A molten carbonate shell modified perovskite redox catalyst for anaerobic oxidative dehydrogenation of ethane, Sci. Adv. 6 (2020) eaaz9339.